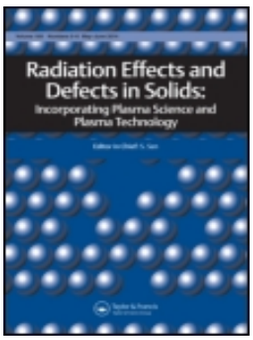

Taylor & Francis
Taylor & Francis Group

Radiation Effects and Defects in Solids
Incorporating Plasma Science and Plasma Technology

ISSN: 1042-0150 (Print) 1029-4953 (Online) Journal homepage: http://www.tandfonline.com/loi/grad20

Effect of suprathermal electrons flux on the ambipolar electric field in stellarators

Julio J. Martinell

To cite this article: Julio J. Martinell (2016) Effect of suprathermal electrons flux on the ambipolar electric field in stellarators, Radiation Effects and Defects in Solids, 171:1-2, 103-108, DOI: 10.1080/10420150.2015.1137917

To link to this article: http://dx.doi.org/10.1080/10420150.2015.1137917

Published online: 09 May 2016.

RADIATION EFFECTS & DEFECTS IN SOLIDS, 2016
VOL. 171, NOS. 1–2, 103–108
http://dx.doi.org/10.1080/10420150.2015.1137917

Taylor & Francis
Taylor & Francis Group

Effect of suprathermal electrons flux on the ambipolar electric field in stellarators

Julio J. Martinell

Instituto de Ciencias Nucleares, UNAM, A. Postal 70-543, México D.F., Mexico

ABSTRACT

Low collisionality plasmas in non-axisymmetric toroidal magnetic devices have significant radial particle fluxes due to trapped particles in the magnetic ripples. The associated ambipolar radial electric field cannot be quantitatively reproduced by standard neoclassical models since the measured values are systematically larger. Here the contribution of suprathermal electrons is included in the radial electric field. The radial flux of suprathermal particles is calculated following a kinetic analysis of the particle transport in which a non-Maxwellian velocity distribution is assumed for the high velocity electrons in the low collisionality regime. The electric field modification produced by the suprathermal electrons is then obtained and an analytical expression for the radial electric field is found which is compared with the one obtained from the thermal particles. An estimate of the needed contribution of the suprathermal electrons is given. Experimental data of the TJ-II Heliac-stellarator are taken for the computations since good Heavy Ion Beam Probe measurements are available.

ARTICLE HISTORY
Received 16 October 2015
Accepted 27 December 2015

KEYWORDS
kinetic theory; transport; magnetic confinement

1. Introduction

In stellarators and other non-axisymmetric toroidal magnetic configurations the neoclassical transport is not intrinsically ambipolar as it is in tokamaks. The main contribution to the difference in the fluxes of electrons and ions in low collisionality plasmas is due to the particles trapped in the magnetic ripples that result from the toroidal asymmetry. These particles experience a radial grad-*B* drift that efficiently takes them out to the plasma edge which is larger for electrons. The non-ambipolar fluxes give rise to a radial electric field over the whole plasma cross section which in turn affects the particle fluxes. The electric field can be measured with different diagnostics like for instance a Heavy Ion Beam Probe (HIBP). Neoclassical transport models can be used to compute the ambipolar electric field by imposing the ambipolarity condition, but these results generally give values that are systematically smaller than those measured by HIBP (*1*, *2*). A similar problem arose in W7-AS where extremely high values of the electron root of the electric field were measured broadening the electron cyclotron resonance heating (ECRH) deposition profile. This was explained in terms of the presence of suprathermal electrons (*3*) created by the very ECRH

CONTACT Julio J. Martinell martinel@nucleares.unam.mx

heating system, that drift out in the local ripples. The same mechanism can be the cause of the larger experimental electric field since suprathermal electrons are always present as ECRH is used in most stellarators which are pumped out to the outer plasma. In this work we consider the presence of these electrons and calculate the electric field produced by the total population of electrons and ions. A kinetic description of the particle transport is followed in which a non-Maxwellian velocity distribution is assumed for the electrons having a high velocity component. For the thermal particles, fluxes are computed from previous expressions proposed by Kovrizhnykh (*4*). The high energy electron contribution to the flux is obtained by accounting the suprathermal electrons with an appropriate tail distribution function. An analytical expression for the electron fluxes is thus found which is used to obtain the ambipolar radial electric field. The resulting electric field turns out to be larger than the one obtained for the thermal plasma, as expected, and the experimental values can be matched when the population of suprathermal electrons is less than 1%.

2. Calculation of the electron flux

The first step is to compute the suprathermal contribution to the electron flux Γ_s. When this is added to the thermal electron flux the relevant ambipolarity condition that has to be solved for the electric field takes the form

$$\Gamma_i = \Gamma_e + \Gamma_s. \tag{1}$$

In order to obtain the macroscopic flux of suprathermal electrons it is necessary to start from kinetic theory. The drift kinetic equation is used together with a model collision operator applied to a magnetic geometry characteristic of a stellarator. Only suprathermal electrons are considered since it is assumed that thermal electrons and ions are described by the existing theories. Since high energy electrons have low collision frequencies it is possible to restrict the analysis to this regime. In the collisionality range contained between the bounce frequency in a ripple $\omega_b = \delta^{1/2} v_{the} N/R$ and the drift frequency in a superbanana $\omega_{sb} = v_{the}^2 \delta/\omega_{ce} r^2$ (*i.e.* $\omega_{sb} < \nu_e/\delta < \omega_b$) the thermal particle fluxes are given by (*5*, *6*)

$$\Gamma_j = -A(\alpha) n_j \left(\frac{T_j}{eBR}\right)^2 \frac{a_j}{\nu_j}\left[\frac{n_j'}{n_j} + b_j \frac{T_j'}{T_j} + e_j \frac{\Phi'}{T_j}\right], \tag{2}$$

where $A(\alpha)$ is a geometric coefficient that depends on the ripple parameter $\alpha = \epsilon/qN\delta$, ν_j the collision frequency and $a_i = 27.42$, $a_e = 12.78$, $b_i = 3.37$, $b_e = 3.45$. Here the magnetic field is modeled by a single harmonic: $B \approx B_0[1 - \epsilon \cos\theta - \delta \cos N\varphi]$.

For the suprathermal particles, the same B-field model is used. The drift kinetic equation with a momentum conserving collision operator $C(f)$ (*7*), for the gyroaveraged function is

$$\frac{\partial f}{\partial t} + (v_\parallel \hat{b} + \mathbf{v}_d)\cdot\nabla f + \frac{\mathrm{d}\mathcal{E}}{\mathrm{d}t}\frac{\partial f}{\partial \mathcal{E}} = C(f) + H(f), \tag{3}$$

where $H(f)$ is a heating term and the collision operator is

$$C_{ei}(f) = \nu_{ei}(K)\frac{v_\parallel}{B}\frac{\partial}{\partial \mu} v_\parallel \frac{\partial}{\partial \mu} f$$

$$C_{ee}(f) = \nu_{ee}(K)\left(\frac{v_\parallel}{B}\frac{\partial}{\partial \mu} v_\parallel \frac{\partial}{\partial \mu} f + v_\parallel \frac{p_e m_e}{T_e} F_0\right)$$

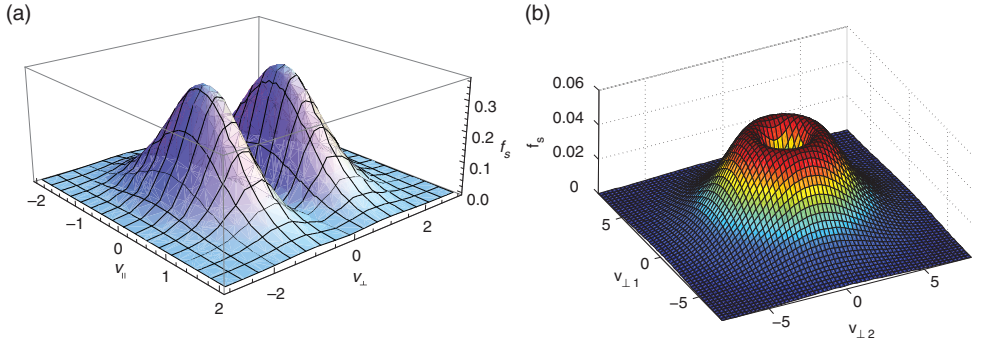

Figure 1. Ring Maxwellian distribution for suprathermal electrons in $v_{\parallel} - |v_{\perp}|$ plane (a) and in $v_{\perp 1} - v_{\perp 2}$ plane (b).

$p_e = T_e \int d^3v \nu_{ee} v_{\parallel} f/(m_e \int d^3v \nu_{ee} v_{\parallel}^2 F_0)$. This is solved for an equilibrium distribution function, $F_0(\mathbf{v})$, of the type expected for suprathermal electrons created by electron cyclotron-heating. In particular, the energy perpendicular to the magnetic field is greatly increased thus creating an anisotropic distribution. The model $F_0(\mathbf{v})$ chosen is a ring Maxwellian in which the maximum in $v_{\perp}$ space is shifted forming a ring. It has the normalized form

$$F_0(\mathbf{r}, \mathbf{v}) = n(\mathbf{r}) \left(\frac{m}{2\pi T_{\parallel}}\right)^{1/2} \frac{m K_{\perp}^p}{2\pi K_s^{1+p} \Gamma(1+p)} \exp(-K_{\parallel}/T_{\parallel}) \exp\left(-\frac{K_{\perp}}{K_s}\right), \tag{4}$$

where $K_{\parallel}$ and $K_{\perp}$ are the components of the kinetic energy, K_s represents the shift in $K_{\perp}$ and measures the energy of suprathermal electrons and p is related to the perpendicular temperature. This function is shown in Figure 1. Since F_0 is assumed to be the zeroth order equilibrium solution, it satisfies $C(F_0) + H(F_0) = 0$. To next order, we write $f = F_0 + \tilde{f}$ and we need to integrate the equilibrium equation at constant energy

$$v_{\parallel} \hat{b} \cdot \nabla \tilde{f} + \mathbf{v}_d \cdot \nabla F_0 = C(\tilde{f}), \tag{5}$$

where the contribution of heating to this order is neglected. The important effect in $C(f)$ comes from pitch angle scattering described by the magnetic moment μ. Standard procedure (*5*, *6*) is used to solve this equation for the low collisionality regime mentioned above, for ripple trapped electrons, leading to

$$\tilde{f} = (\sin\theta_0 / eR\nu)(\mu - \mu_m) F_0',$$

where θ_0 labels filed lines, $\mu_m = K/B_{\max}$ at maximum turning point and $\nu = \nu_{ee}(K) + \nu_{ei}(K)$.

From $\tilde{f}$ the electron flux is computed integrating in angles, K and μ obtaining the result

$$\Gamma_s = -A(\alpha) n_s \left(\frac{T_{\parallel}}{eBR}\right)^2 \frac{c_1}{\nu_e} \left[\frac{n_s'}{n_s} - \frac{T_{\parallel}'}{2T_{\parallel}} - e\frac{\Phi'}{T_{\parallel}} + \left(\frac{c_2}{\hat{K}} - 2\right)\frac{\hat{K}'}{\hat{K}}\right], \tag{6}$$

where $A(\alpha)$ is the same geometrical coefficient in Equation (2), $\hat{K} = K_s/T_{\parallel}$ represents the energy of suprathermal electrons relative to parallel thermal energy and the coefficients c_1

Table 1. Values of the coefficients c_1, c_2 for some values of the parameters of the ring Maxwellian distribution function.

	c_1			c_2		
$\hat{K}_M \backslash p$	2	3	4	2	3	4
1	63.14	187.8	435.6	5.95	6.96	7.96
2	984.7	2941.5	6842.6	11.95	13.96	15.96
3	4942.7	14786	34430	17.95	20.96	23.96

and c_2 are

$$c_1 = \frac{I_1^p}{\hat{K}^{1+p}\Gamma(1+p)}, \quad c_2 = \frac{I_2^p}{I_1^p}, \quad I_n^p = \int_0^\infty \frac{x^{3+p+n}\,\mathrm{e}^{-x/\hat{K}}\,\mathrm{d}x}{H(x)}, \quad \eta(x) = \frac{2}{\sqrt{\pi}}\int_0^x \mathrm{e}^{-t}t^{1/2}\,\mathrm{d}t$$

and $H(x) = \eta(x) + \eta'(x) - \eta(x)/2x + \eta(\hat{x}) + \eta'(\hat{x}) - \eta(\hat{x})/2\hat{x}$, $\hat{x} = m_i/m_e x$ comes from the energy dependence of collision frequency. They are computed numerically for a constant value of $\hat{K}(r)$ (taken as its maximum $\hat{K}_M$). Some of their values are given in Table 1 for $\hat{K}_M = 1, 2, 3$ and $p = 2,3,4$. It is noticed that the flux increases strongly as the energy of the supathermal electrons gets larger.

3. Ambipolar electric field

The significance of the expression presented above for the suprathermal electrons flux can be estimated by the way it modifies the radial electric field. This flux can be used in the extended ambipolarity condition Equation (1) in order to find the resulting ambipolar electric field. Since the transport coefficients here do not depend on the electric field, as it occurs in more elaborate models that cover different collisionality regimes (*4*), it is easy to solve Equation (1) together with Equations (2), (6) for the radial electric field $E_r = -\Phi'$. This simple estimate gives

$$E_r = -\frac{T_e}{e}\frac{\frac{n'}{n}(1 - 2.1m_r t^{7/2}) + 3.4\frac{T_e'}{T_e} - 7.3\frac{T_i'}{T_i}m_r t^{7/2} + \frac{c_1}{12.8}f_s\frac{T_\parallel^2}{T_e^2}\left(\frac{n_s'}{n_s} - \frac{T_\parallel'}{2T_\parallel} + \frac{\hat{K}'}{\hat{K}}\left(\frac{c_2}{\hat{K}} - 2\right)\right)}{1 + 2.1m_r t^{5/2} + \frac{c_1}{12.8}f_s T_\parallel/T_e}, \tag{7}$$

where $f_s(r) = n_s/n$, $t(r) = T_i/T_e$, $m_r = \sqrt{m_i/m_e}$. Since all plasma parameters vary with radius the expression provides a way to compute the radial electric field profile when the radial dependencies of the other quantities are provided. For the calculations we use typical profiles for the TJ-II Heliac-stellarator since good measurements of the radial electric field are available with HIBP. Typical experimental density and temperature profiles are fitted using polynomials of the form: $n(r) = n_b + n_0(1 - x^a)^b$ and $T_j(r) = t_b + t_0(1 - x^c)^d$ for different line densities. First, in Figure 2(a) we show the fitted n and T_j profiles used and the resulting electric field profiles for four line averaged densities with no suprathermal population ($f_s = 0$). The $E_r(\rho)$ are not exactly like the profiles measured by HIBP, due to the restriction of low ν_e, but they reproduce the main features like positive E_r at low n and completely negative E_r for high n.

In order to include suprathermal particles it is necessary to give profiles for n_s, $T_\parallel$ and $\hat{K}$. For these we assume on-axis heating so that the $n_s(r)$ and $\hat{K}(r)$ are centrally peaked and very

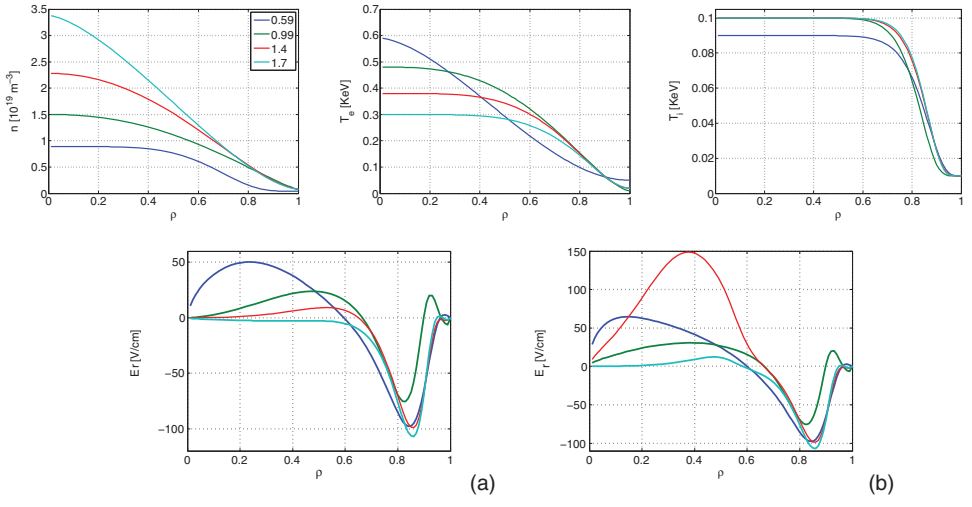

Figure 2. n and T_j profiles for 4 line-averaged densities (given in the legend in units of 10^{19} m^{-3}) and respective E_r profiles (a) with only thermal particles (b) with 1% of suprathermal electrons. Low $\bar{n}$ is blue (top curves).

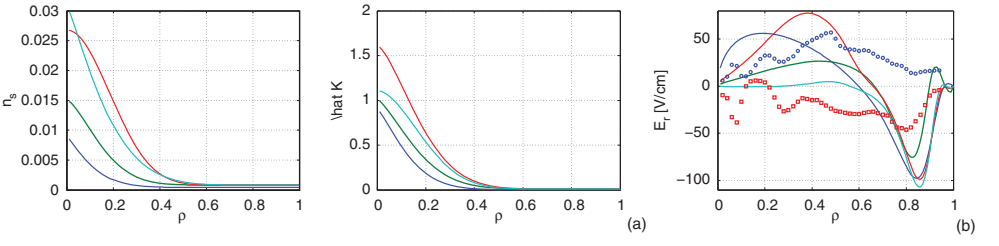

Figure 3. (a) Profiles for suprathermal electrons parameters n_s and $\hat{K}$. (b) E_r profile for 0.5% of energetic electrons; experimental E_r profiles are shown with the symbols for low (circles) and high densities (squares).

narrow with a half mean width $\Delta \leq a/5$ as pictured in Figure 3(a). For the parallel temperature we assume it is similar to the thermal electrons $T_{\|} \approx T_e$. The suprathermal population is taken as 1% of the main density ($f_s \sim 0.01$) with $0.9 \leq \hat{K}_M \leq 1.6$ and $p = 2$. The corresponding electric field profiles are shown in Figure 2(b) for the same densities used for thermal particles. It can be appreciated that the magnitude of E_r can be increased substantially, especially for the inner regions at low densities. For the high densities, the electric field can even become positive and it is no longer all negative. As expected, the effect is less important near the edge since the suprathermal population is negligible there. Notice that the effect of increasing $\hat{K}$ is quite strong since for the density $\bar{n} = 1.4 \times 10^{19}$ we took $\hat{K}_M = 1.6$ (see Figure 2(a)) and this causes E_r to rise to $\approx$ 150 V/cm. For comparison, in Figure 3(b) the $E_r(r)$ with the lower suprathermal population of 0.5% is shown, having a moderate increase of E-field values, which is closer to reality. There we also show the experimental profiles from HIBP corresponding to the two extreme densities for a typical discharge of TJ-II (# 15855) (*2*) just as a reference. As seen, the magnitude of E_r can be matched although the shape of

the profiles differs. The behavior is not accurate since at high densities the plasma is more collisional and our calculations for low collisionality are not applicable.

4. Conclusions

A radial flux is obtained for a non-thermal distribution of electrons from kinetic theory having novel dependencies. The result reflects the assumed form of the ring Maxwellian distribution. The electric field obtained when the suprathermal flux is included provides better agreement with experiment than for the thermal plasma since the values are increased where fast electrons are present. This is a natural result since an increased total electron flux gives rise to positive electric fields. The population of suprathermal electrons should be of the order of 0.5% in order to match experimental values. More accurate computations are needed in order to compare with the experimental measurements which must include equations for Γ_s at higher collisionalities. A more adequate computation should include the evolution of the suprathermal population according to a transport model in order to better compare with experiment.

Disclosure statement

No potential conflict of interest was reported by the author.

Funding

This work was partially supported by DGAPA-UNAM IN109115 and CONACyT 152905 projects.

References

(1) Dinklage A.; Yokoyama, M.; Tanaka, K.; Velasco, J.L.; López-Bruna, D.; Beidler, C.D.; Satake, S.; Ascasíbar, E.; Arévalo, J.; Baldzuhn, J.; Feng, Y.; Gates, D.; Geiger, J.; Ida, K.; Isaev, M.; Jakubowski, M.; López-Fraguas, A.; Maaßberg, H.; Miyazawa, J.; Morisaki, T.; Murakami, S.; Pablant, N.; Kobayashi, S.; Seki, R.; Suzuki, C.; Suzuki, Y.; Turkin, Yu.; Wakasa, A.; Wolf, R.; Yamada, H.; Yoshinuma, M. *Nucl. Fusion* **2013,** *53,* 063022.
(2) Gutiérrez-Tapia C.; Martinell, J.J.; López-Bruna D.; Melnikov, A.V.; Eliseev, L.; Rodríguez, C.; Ochando, M.A.; Castejón, F.; García, J.; van Milligen, B.P.; Fontdecaba, J.M. *Plasma Phys. Control Fusion* **2015,** *57,* 115004.
(3) Murakami, S.; Gasparino, U.; Idei, H.; Kubo, S.; Maassberg, H.; Marushchenko, N.; Nakajima, N.; Romé, M.; Okamoto, M. 1999. *17th IAEA Fusion Energy Conference*, Yokohama, TH2/1.
(4) Kovrizhnykh, L.M. *Plasma Phys. Rep.* **2006,** *32,* 988–995.
(5) Connor, J.W.; Hastie, R.J. *Nucl. Fusion* **1973,** *13,* 221–225.
(6) Kovrizhnykh, L.M. *Nucl. Fusion* **1984,** *24,* 851–936.
(7) Hirshman, S.P.; Sigmar, D.J. *Phys. Fluids* **1976,** *19,* 1532–1540.